

## Modification in morphological, structural, photoluminescence and antibacterial properties of SnS and CdS thin films by cold plasma treatment

A. A. Khadayeir<sup>a</sup>, F. A. Najim<sup>a,\*</sup>, A. H. Wanas<sup>a</sup>

*Department of Physics, College Of Educations, University of Al-Qadisiyah, 58002, Iraq*

SnS and CdS thin films was synthesized by electrochemical method and then the effect of applying the cold plasma on its properties was investigated. The morphology and structural properties of thin films were studied before and after plasma treatment using X-ray diffraction spectrum, field-effect scanning electron microscope, energy dispersive X-ray spectrum, Time-resolved photoluminescence and atomic force microscope. Given the high potential of cold plasma in surface modification of materials, the amount of wettability and antibacterial properties of thin films in the presence of standard gram-positive and gram-negative bacteria was compared before and after plasma treatment. Results show that the applying the plasma causes the significant changes in morphology, self-cleaning and antibacterial properties of SnS and CdS thin films.

(Received April 19, 2021; Accepted July 6, 2021)

*Keywords:* Plasma treatment, Cold plasma, SnS, CdS, TRPL, Antibacterial, Wettability

### 1. Introduction

Atmospheric pressure plasma jets (cold plasma) have gotten a lot of attention in recent years because of their wide range of applications in plasma assisted combustion, material processing, and plasma assisted biomedical applications[1]

Semiconducting metal chalcogenides have received much attention in recent years for their wide applications [2-6]. These applications include solar cells, sensors, photovoltaic and photo-electronic components, photo-detectors and field-effect transistors [7-12]. Among the semiconducting metal chalcogenides, tin sulfide has received much attention due to large optical absorption coefficient with high photo-electric conversion efficiency [13-14] and cadmium sulfide have received a lot of attention due to large optical gap (2.4eV) [15-16]. Tin sulfide is an IV-VI semiconductor that is formed in the orthorhombic phase ( $a=0.399\text{nm}$ ,  $b=0.434\text{nm}$ ,  $c=1.12\text{nm}$ ). Tin sulfide also has a zinc blende phase ( $a=0.5845\text{nm}$ ). The cell unit of tin sulfide has two layers that are formed along the c-axis of the crystal. The optical band gap reported for tin sulfide is between 1.1-2.1eV [17-19]. Cadmium sulfide has three different crystal phases: hexagonal (wurtzite), cubic (zinc-blende), rock salt, which is a combination of hexagonal and cubic phases. The hexagonal phase is thermodynamically more stable than other phases [20-21].

Many methods have been developed for deposition these structures such as sputtering, molecular beam epitaxy, thermal evaporation, chemical bath deposition, successive ionic layer adsorption and reaction, spray pyrolysis, and electro deposition [22-30]. Most researches have used post-deposition treatment to improve the properties of thin films. But plasma treatment seems to be a better way to modify the structural, physical and biological characteristics of the thin films. Therefore, in the research, in order to improve the self-cleaning and antibacterial properties of SnS and CdS thin films, the surface of the samples was activated through plasma treatment in air under operating power of 1kW.

---

\* Corresponding author: [firmas.najim@qu.edu.iq](mailto:firmas.najim@qu.edu.iq)

## 2. Experimental details

Electrochemical methods were used to synthesize SnS and CdS thin films. Plasma treatment: the surface of thin films is activated through plasma treatment and the surface roughness created on them prepares the surfaces for future operations. The distance of the plasma head from the samples is about 4 cm. The power of the device is 1 kW, the operating frequency is 20 kHz and the applied gas is air. Coating of the desired solution begins evenly on the surface. Plasma surface pretreatment leads to better absorption and adhesion of the solution in the coating stage. The samples were coated with nano-silver antibacterial solution at a concentration of 200 ppm. In the next stage, the samples are entered into the dryer and their cooking and drying operations are performed. It was the radiant dryer and the samples were dried at 200 °C. The cold plasma system shown in Fig. 1.

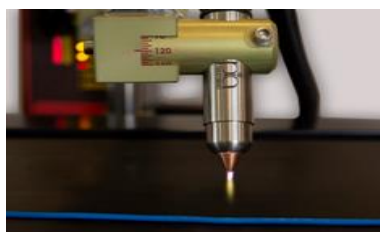


*Fig. 1. The cold plasma system.*

X-ray diffraction (XRD) was determined by using D8 Advance Bruker YT model and  $\text{CuK}_\alpha$  radiation was used to confirm the structure of SnS and CdS thin films. A field-emission scanning electron microscope (FESEM), MIRA3 TESCAN-XMU model equipped with EDX analysis was used to inspect the chemical analysis and surface morphology of the films. AFM images obtained from atomic force microscope (AFM) device, manufactured by Ara-Research Company, were used to investigate the surface topology of the films. In order to measure the self-cleaning properties of the samples, the contact angle of water droplets with 1  $\mu\text{L}$  volume on tin sulfide and cadmium sulfide thin films in ambient conditions at 25 °C was measured using AM-7013MZT, Dino-Lite, Taiwan. The water droplets were placed at 3 different positions for one sample and its average was considered as the contact angle. In order to measure the antibacterial properties, the gram-negative bacterium of *Escherichia coli* DH5 alpha and gram-positive of standard *S. aureus* (ATCC 25922) (1399PTCC).

## 3. Results and discussion

### 3.1. Structural Analysis Using XRD

X-ray diffraction spectrum is used to investigate the structural composition and fuzzy analysis of materials. Measurement of X-ray diffraction spectrum of SnS and CdS thin films before and after applying the plasma was performed using Bruker D8 advanced Diffractometer. X-ray spectrum of the samples was measured using  $\text{CuK}_\alpha$  radiation at 1.5418 Å in the range of 5° to 80°. X-ray diffraction spectrum of SnS thin film before applying the plasma (black) and after applying the plasma (red) is shown in Fig. 2 a and b.

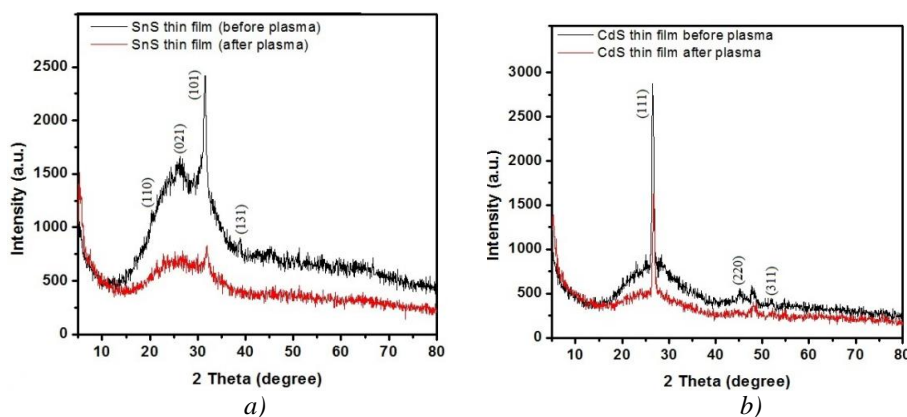


Fig. 2. X-Ray Diffraction Spectrum of a) SnS Thin Film before Applying the Plasma (Black) and after Applying the Plasma (Red), b) CdS Thin Film before Applying the Plasma (Black) and after Applying the Plasma (Red).

Comparison of diffraction spectrum obtained by JCPDS card No.039-0354 shows that the structure of SnS is composed of an orthorhombic phase (mineral herzenbergite) and the main peaks are located at angles of 20.54, 26.49, 31.48, 38.89, corresponding to the planes of (110), (021), (101), (131), respectively [31-33]. The peak height of the (101) plane has the most intensity compared to the other peaks, indicating that the preferred orientation of SnS thin film before applying the plasma is along the (101) plane. After applying the plasma, the intensity of all peaks is significantly reduced, although the preferred orientation is still in the direction of the (101) plane.

The diffraction spectrum of CdS thin film before and after applying the plasma is shown in Fig. 1b. The analysis of diffraction spectrum shows that the main peak is located at an angle of 26.47°, which corresponds to the (111) plane and confirms the formation of cubic phase of CdS (JCPDS card No. 89-0019) [34-35]. The preferred orientation for the growth of the structure is along the (111) plane. Other peaks which are located at angles of 45.18, 47.98, 51.84 have very low intensity. The amplitude of the peaks is greatly decreased by applying the plasma, similar to the SnS thin film.

### 3.2. Investigation of Structure Morphology Using FESEM

The microstructure and surface morphology of CdS and SnS thin films were investigated using the field-emission scanning electron microscope (FESEM), MIRA3TESCAN-XMU model. The results obtained for the thin films before and after applying the plasma are reported in Fig. 3. The voltage used to capture these images was 10kV. Fig. 3a., which is related to tin sulfide thin film before applying the plasma, shows that the structure of SnS crystallites is in the form of blades with a length of about 200nm and a diameter of about 20-30nm. By applying the plasma, no change is seen in the structure of the crystallites, as shown in Fig. 3b.

The structure of CdS thin film before and after applying the plasma is shown in Fig. 3c and 3d. Cadmium sulfide nano-particles are seen in the form of small spheres in the Figure, most of which are bonded together and agglomerated. After the applying the plasma, the bonding between them increases and they form an almost uniform surface. Cross-section image of SnS and CdS thin film samples before and after applying the plasma are shown in Fig.4. The cross-section area of SnS thin film has not changed much, as shown in FESEM image. However, in the case of CdS thin film, after the applying the plasma, the particles are completely bonded together, which is also clearly visible in the cross-section image.

(FESEM) and (EDX) system was used to scrutinize the elements in the films. The voltage used to perform these tests ranged from zero to 10kV. The results of energy-dispersive X-ray spectroscopy of SnS and CdS thin films before and after applying the plasma are shown in Fig. 5. X-ray energy diagrams are drawn based on the proportion of X-ray energy received from each energy level. Each of the peaks in these diagrams corresponds to a particular atom. The specific elements in the results of the (EDX) test are also fully expected and confirm the successful

synthesis of these compounds. In SnS thin film, elements of tin and sulfur are only seen. In CdS thin film, cadmium and sulfur atoms are only seen and no impurity element is seen.

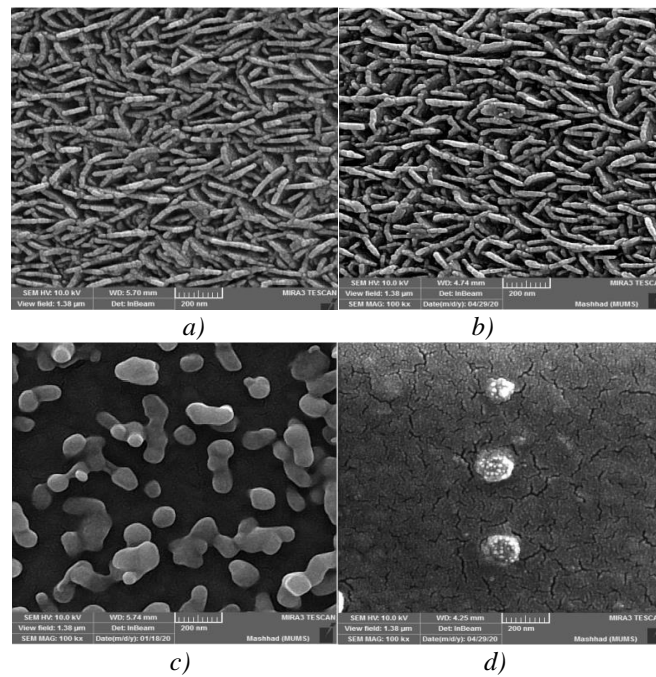


Fig. 3. a) FESEM Image of Tin Sulfide Thin Film before Applying the Plasma, b) Tin Sulfide Thin Film after Applying the Plasma, c) Cadmium Sulfide Thin Film before Applying the Plasma, d) Cadmium Sulfide Thin Film after Applying the Plasma.

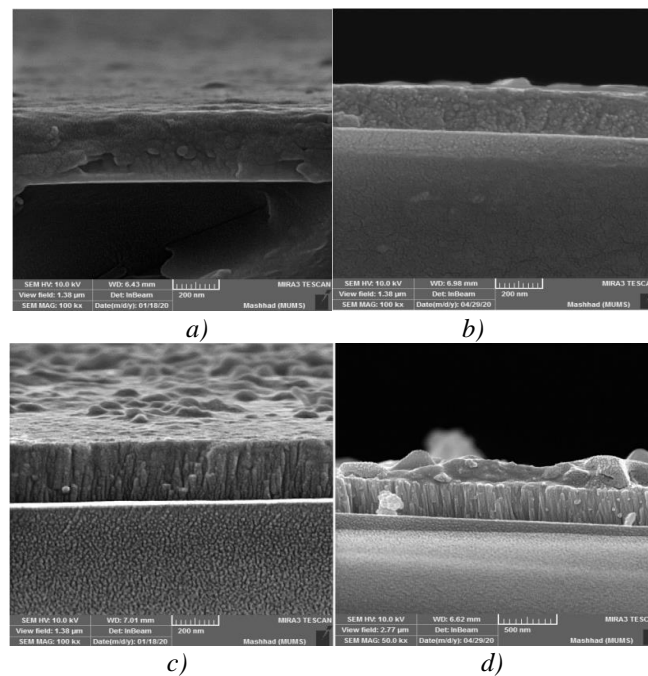


Fig. 4. Cross-section Area Image of a) Tin Sulfide Thin Film before Applying the Plasma, b) Tin Sulfide Thin Film after Applying the Plasma, c) Cadmium Sulfide Thin Film before Applying the Plasma, d) Cadmium Sulfide Thin Film after Applying the Plasma.

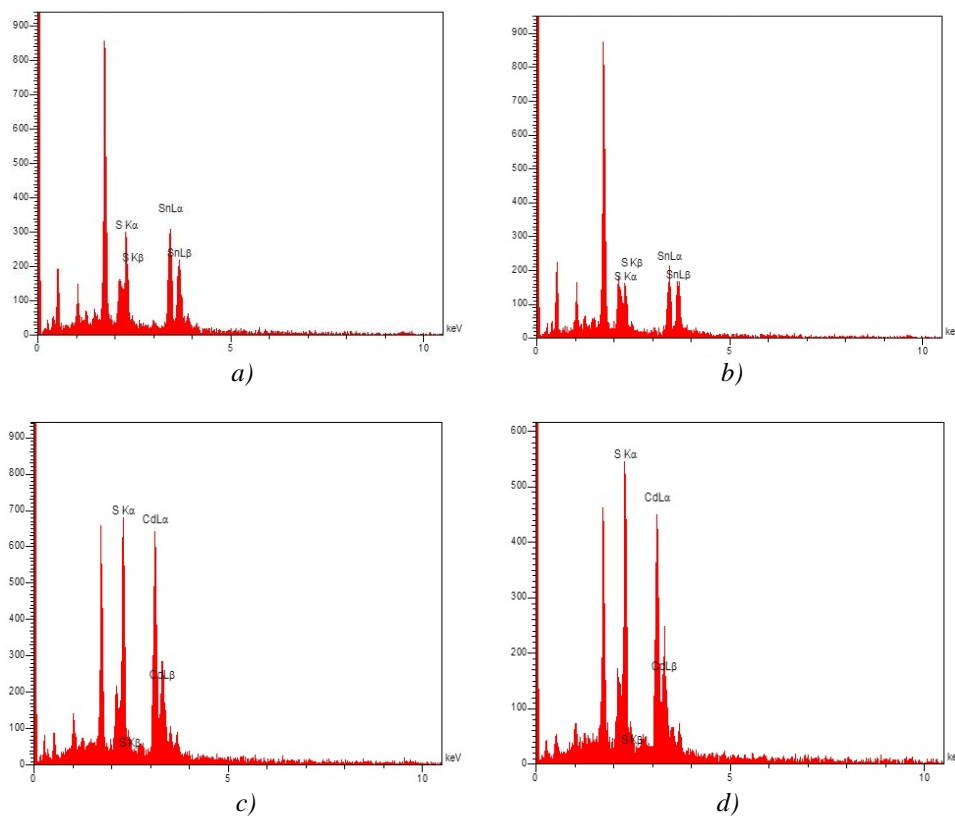


Fig. 5. EDX Diagram of a) Tin Sulfide Thin Film before Applying the Plasma, b) Tin Sulfide Thin Film after Applying the Plasma, c) Cadmium Sulfide Thin Film before Applying the Plasma, d) Cadmium Sulfide Thin Film after Applying the Plasma.

### 3.3. Time-Resolved Photoluminescence

Time-resolved photoluminescence (TRPL) has been proposed as a useful method for measuring the photovoltaic materials of thin film with a direct band gap in the visible or near-infrared range.

TRPL measurements are designed to detect the photons emitted from a sample by radiative recombination. Higher extinction efficiency of PL in the hole transmission of SnS indicate that hole extraction is more efficient, and was further confirmed by experiments (TRPL). Fig.6 shows the PL reduction for SnS thin films before and after plasma-surface adjustment.

Before the plasma is applied, a rapid reduction in PL is observed on the surface of the SnS thin film, followed by a gradual reduction due to the presence of unauthorized carriers in SnS films and the charge carriers' slow diffusion. SnS thin film after plasma-surface modification has a long average lifetime with a rapid reduction time constant, indicating a high quality SnS thin film after plasma-surface modification with low trap density. In order to better understand the quantitative idea of the recombination mechanism of carriers, a TRPL test was taken from CdS thin film before and after plasma treatment, as can be seen in Fig. 7, which can be used to estimate the effective reduction time. The corresponding photon energy (1.65eV) of the laser excitation is lower than the band gap energy of CdS (2.42eV). Therefore, light is transmitted through these layers.

Before plasma modification, a slow reduction in PL is observed on the surface of CdS thin film. CdS thin film after plasma-surface modification has a long lifetime with a rapid reduction time constant, which indicates a high quality CdS thin film after plasma modification [36-39].

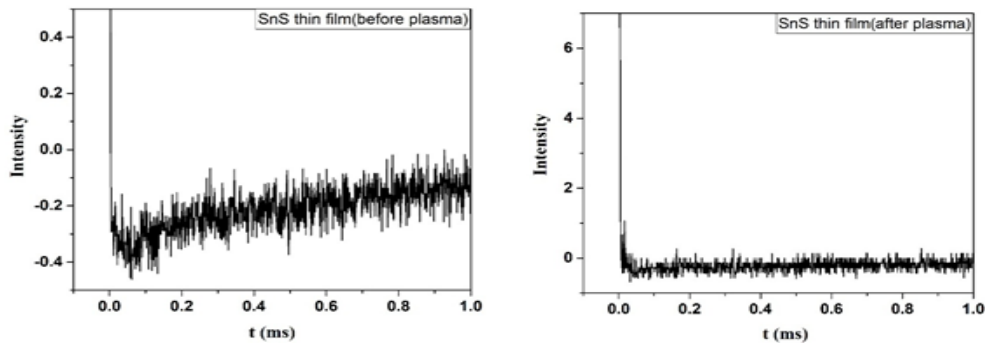


Fig. 6. TRPL for SnS Thin Film before and after Plasma Treatment.

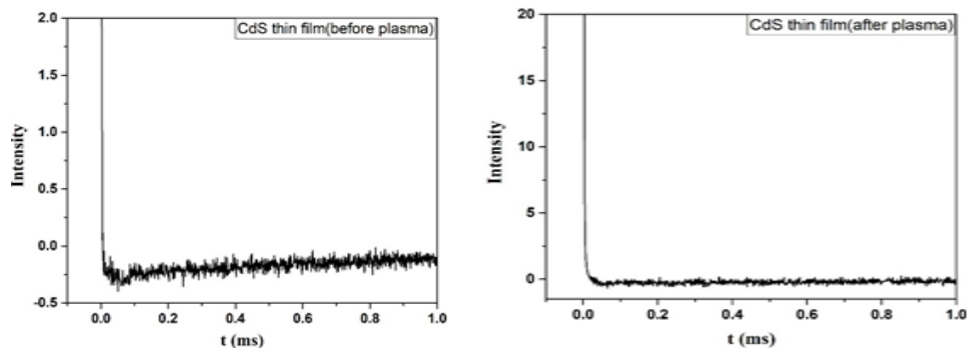


Fig. 7. TRPL for CdS Thin Film before and after Plasma.

### 3.4. Investigation of Surface Topology Using AFM

Fig. 8 (a-d) shows the 2D and 3D AFM images of surface topology for SnS thin film before and after plasma treatment. Fig. 8a shows the AFM 2D image of SnS thin film. In the Fig. 8b., well-grown grains with an average particle size of 265 nm are observed. Larger grain sizes can reduce the dispersion of charge carriers at grain boundaries and help improve the efficiency of solar cell devices. To prevent recombination of minority carriers at grain boundaries, it is desirable to have the larger lateral grain size compared to the propagation length of the lateral carriers. The root-mean-square value of the surface smoothness of the deposited thin films is 19.83 nm, which is very high compared to SnS single crystals and thin films grown by other methods [40, 41]. A layer can minimize the total energy by keeping its surface area as small as possible (i.e., ideally flat).

While SnS thin film has the compacted small grains with a smooth surface, after plasma jet treatment, SnS thin film shown in Fig. 8C is composed of much larger grains with much higher porosity. It is clear that due to the porosity, it increases throughout the surface area, thus increasing the scattering and penetration of light. In addition, larger grains prevent the inverse recombination of electron-hole pairs. Analysis of AFM 3D images after plasma treatment is shown in Fig. 8d.

Fig. 9(a-d) shows the 2D and 3D AFM images of CdS thin film before and after plasma treatment. CdS surface shown in Fig. 9a. is continuous and compact, and there are some nanoparticles on the top layer that can effectively enhance the light absorption. The grain sizes determined by AFM images is consistent with the results obtained from XRD measurements. AFM 3D image is shown in Fig. 9b. [42].

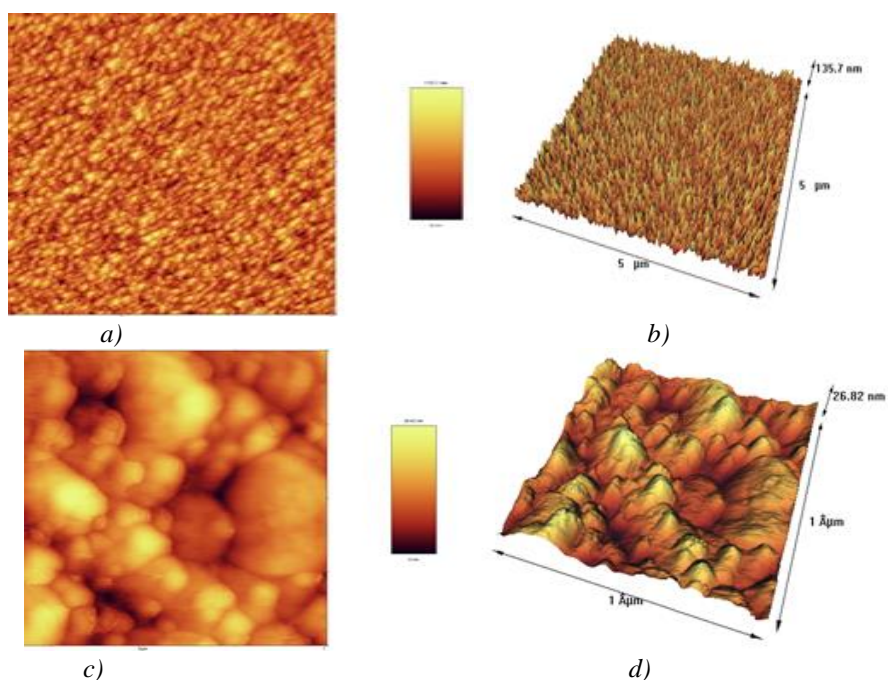


Fig. 8. AFM Images of SnS Thin Film of a) 2D before Plasma Treatment, b) 3D before Plasma Treatment, c) 2D after Plasma Treatment, d) 3D after Plasma Treatment.

Two-dimensional and three-dimensional AFM images of CdS thin film deposited on a glass substrate after plasma treatment are shown in Fig. 9a. and b. The size of other particles calculated by AFM images in the thin film was 50nm. Non-uniform distribution of clusters and porosity are observed in the film. This may reduce the film density. This non-uniform distribution of clusters creates the top and bottom alignment of most crystals, which increases the film roughness by 90nm.

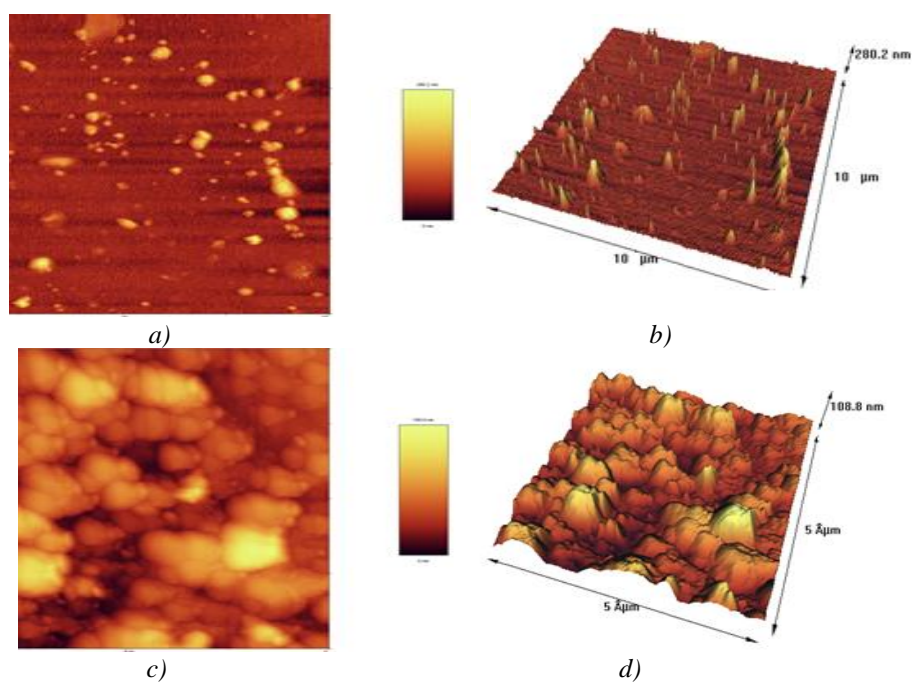


Fig. 9. AFM Images of CdS Thin Film of a) 2D before Plasma Treatment, b) 3D before Plasma Treatment, c) 2D after Plasma Treatment, d) 3D after Plasma Treatment.

### 3.5. Wettability Studies (Contact Angle Measurement)

Wettability test is performed to investigate the interaction between water and the surface of the thin film. The wetting behavior of the surface is determined by a microscopic parameter called the contact angle (CA), which involves measuring the contact angle between water and the thin film. Wetting of a surface occurs when  $CA < 90^\circ$  and non-wetting occurs when  $CA > 90^\circ$ , and accordingly, are called hydrophilic and hydrophobe, respectively [43 , 44].

Fig. 10a and 10b show the image of wetting of SnS thin film surface before and after plasma treatment. As can be observed, SnS thin film has a contact angle of  $76.6^\circ$  before plasma treatment Fig. 10a, indicating the hydrophilicity of SnS thin film surface. In comparison, after plasma surface treatment, the surface of SnS thin film becomes hydrophobic Fig. 10b. The contact angle of SnS thin film exposed to the plasma is  $108^\circ$ . This plasma treatment usually reduces the surface defect, thus changing the surface from hydrophilic (hydrophilicity) to hydrophobic (hydrophobicity).

Plasma treatment activates the substrate surface by increasing the surface energy. The surface energy of the material was tested by measuring the contact angle with water before and after plasma treatment in CdS thin film. Fig. 11a and 11b show the effect of plasma treatment on CdS surface. The contact angle that the droplet forms with the surface of CdS thin film is about  $72^\circ$  before plasma treatment, and as shown in Fig. 11b, the contact angle after plasma treatment is about  $94^\circ$ .

As can be seen from the Figure, plasma treatment somewhat reduces the hydrophilic behavior, but still shows the hydrophilic behavior. Increasing the surface energy is useful for the adhesion and durability of the thin film. Increasing the surface energy may alter the growth kinetics of thin film. However, ellipsometric spectroscopy which detect a slight difference in thin film thickness for layers deposited on plasma treated and untreated surfaces, which is measured by

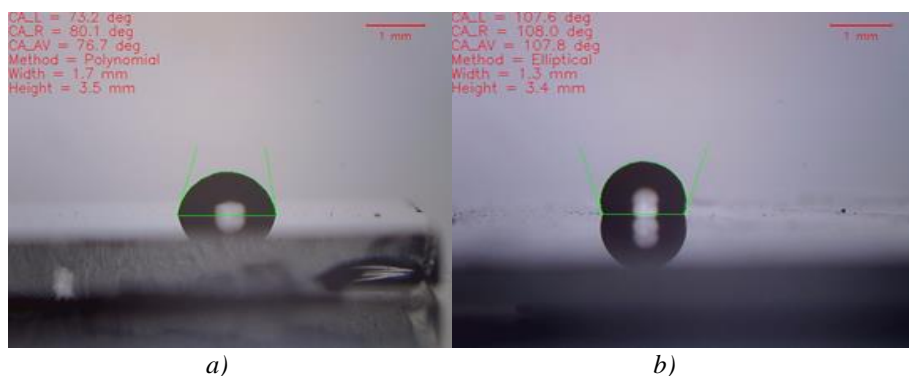


Fig. 10a-b. The Images of Angle Contact of SnS Thin Film a) before Plasma Treatment, b) after Plasma Treatment.

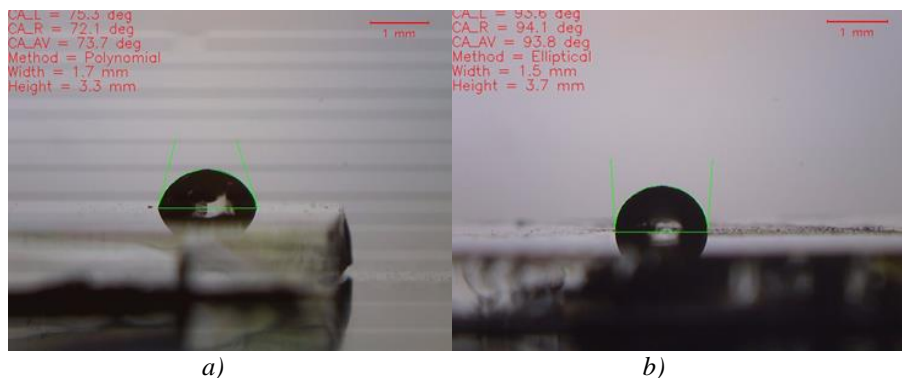


Fig. 11a-b. The Images of Angle Contact of CdS Thin Film a) before Plasma Treatment, b) after Plasma Treatment.

### 3.6. Antibacterial Activity

The antibacterial properties of SnS thin film were investigated before and after plasma treatment. The results of experiments on *S. aureus* and *E. coli* for 24 hours on empty glass substrates and SnS thin film surfaces incubated before and after plasma treatment are shown in Fig. 12 and 13. Plasma jet treatment has already been shown to inhibit the growth of both bacteria on hard surfaces and in liquid environments [45-49]. Therefore, the effect of plasma jet treatment on both gram-positive and gram-negative bacteria has been investigated. As shown in Fig. 12, the growth of *Staphylococcus* in SnS thin film was inhibited by 10% before plasma treatment compared to the control sample, while the growth of this bacterium after plasma treatment and exposure to the plasma flow showed a mild reduction and was inhibited by 50% compared to the control sample. The antibacterial properties for *E. coli* in SnS thin film are also measured before plasma treatment and are shown in Fig. 13. As can be seen, this film does not have the antibacterial properties compared to the control sample before plasma treatment.



Fig. 12. Antibacterial Test on *Staphylococcus* in Thin Film of a) SnS before Plasma Treatment, and b) SnS after Plasma Treatment



Fig. 13. Antibacterial Test on *E. coli* in Thin Film of a) SnS before Plasma Treatment, and b) SnS after Plasma Treatment.

For CdS thin film before and after plasma treatment, antibacterial properties and the percentage of the growth inhibition for *Staphylococcus* are also measured and shown in Fig. 14 and 15. As can be seen from Fig. 14, the percentage of growth inhibition before plasma treatment was 10% compared to the control sample, while the growth of this bacterium after plasma treatment and exposure to the plasma flow decreased sharply compared to the control sample and was inhibited by 90%. In the case of *E. coli* in CdS thin film, the antibacterial test is measured before and after plasma treatment and is shown in Fig. 15. As can be seen, before plasma treatment, the percentage of growth inhibition compared to the control sample was about 10%, while after plasma treatment, the percentage of growth inhibition reached 90%, showing that the thin film surface treatment by plasma jet has a good effect on inhibiting the growth of this bacterium.



Fig. 14. Antibacterial Test on Staphylococcus in Thin Film of a) CdS before Plasma Treatment, and b) CdS after Plasma Treatment



Fig. 15. Antibacterial Test on E.coli in Thin Film of a) CdS before Plasma Treatment, and b) CdS after Plasma Treatment.

#### 4. Conclusion

SnS and CdS thin films were synthesized and deposited using an electrochemical process in this study. The surface of SnS and CdS thin films were treated with cold plasma with 1kW power in the presence of air and at 200°C, and the samples were characterized before and after applying the plasma. Examining the X-ray diffraction spectrum confirms the formation of the desired phases. XRD spectrum did not change much before and after applying the plasma. According to the results of XRD and EDX, no impurity phase is observed in the samples. Morphology and surface of samples were investigated using FESEM and AFM microscopes. SnS and CdS thin films after plasma-surface modification have a long average lifetime with a rapid reduction time constant, indicating a high quality SnS and CdS thin films after plasma-surface modification with low trap density.

A study of the contact angle between the water droplet and the surface of the samples shows that the contact angle is increased after plasma treatment. In fact, plasma treatment usually reduces the surface defect, thus changing the surface from hydrophilic to hydrophobic. Analyzing the antibacterial properties of thin films against Staphylococcus and E.Coli bacteria revealed that before plasma treatment, bacterial growth was inhibited by 10% relative to the control sample, but after plasma treatment, a very significant difference was observed, and thin films were able to inhibit bacterial growth by 99%.

#### References

- [1] B. Ghimire, P. Lamichhane, J. S. Lim, B. Min, R. Paneru, K. D. Weltmann, E. H. Choi, Applied Physics letters **113**(19), 194101 (2018).
- [2] R. Caballero, V. Condé, M. León, Thin Solid Films **612**, 202 (2016).
- [3] W. E. Mahmoud, Sensors and Actuators: B Chemical **238**, 1001 (2017).
- [4] F. A. Al-Agel, W. E. Mahmoud, Journal of Applied Crystallography **45**(5), 921 (2012).
- [5] F. A. Al-Agel, W. E. Mahmoud, Materials Letters **82**, 82 (2012).
- [6] H. Li, J. Ji, X. Zheng, Y. Ma, Z. Jin, H. Ji, Materials Science in Semiconductor Processing **36**, 65 (2015).
- [7] J. Z. Ou, W. Ge, B. Carey, T. Daeneke, A. Rotbart, W. Shan, Y. Wang, Z. Fu, A. F. Chrimes, W. Wlodarski, S. P. Russo, Y. X. Li, K. K. Zadeh, ACS Nano **9**(10),

- 10313 (2015).
- [8] J. Wang, G. Lian, Z. Xu, C. Fu, Z. Lin, L. Li, Q. Wang, D. Cui, C.P. Wong, *ACS Applied Materials & Interfaces* **8**(15), 9545 (2016).
- [9] A. Bagheri, M. Sabbaghan, Z. Mirgani, *Spectrochimica Acta Part A: Molecular and Biomolecular Spectroscopy* **137**, 1286 (2015).
- [10] M. N. Amroun, M. Khadraoui, R. Miloua, Z. Kebbab, K. Sahraoui, *Optik* **131**, 152 (2017).
- [11] D. I. Bletskan, *Journal of Ovonic Research* **1**(5), 47 (2005).
- [12] X. Hu, G. Song, W. Li, Y. Peng, L. Jiang, Y. Xue, Q. Liu, Z. Chen, J. Hu, *Materials Research Bulletin* **48**(6), 2325 (2013).
- [13] M. S. Niasari, M. Bazarganipour, F. Davar, A. A. Fazil, *Applied Surface Science* **257**(3), 781 (2010).
- [14] D. Guan, J. Li, X. Gao, Y. Xie, C. Yuan, *Journal of Alloys and Compounds* **658**, 190 (2016).
- [15] J. Britt, C. Ferekides, *Applied Physics Letters* **62**, 2851 (1993).
- [16] T. L. Chu, and S. S. Chu, *Solid-State Electronics* **38**, 533 (1995).
- [17] E. Guneri, F. Gode, C. Ulutas, F. Kirmizigul, G. Altindemir, C. Gumus, *Chalcogenide Letters* **7**(12), 685(2010).
- [18] A. Zehe, J. G. Vazquez Luna, *Solar Energy Materials and Solar cell* **68**(2), 217 (2001).
- [19] J. H. Schon, O. Schenker, B. Batlogg, *Thin Solid Films* **385**(1-2), 271 (2001).
- [20] U. Pal, R. Silva Gonzalez, G. Martinez-Montes, M. Garcia-Jimenez, M. A. Vidal, Sh. Torres, *Thin Solid Films* **305**, 354 (1997).
- [21] K. L. Chopra, S. Major, D. K. Pandya, *Thin Solid Films* **102**(1), 1 (1983).
- [22] M. M. El-Nahass, H. M. Zeyada, M. S. Aziz, N. A. El-Ghamaz, *Optical Materials* **20**(3), 159 (2002).
- [23] B. Subramanian, C. Sanjeeviraja, M Jayachandran, *Materials Chemistry and Physics* **71**(1), 40 (2001).
- [24] C. Gao, H. Shen, L. Sun, Z. Shen, *Materials Letters* **65**(9), 1413 (2011).
- [25] B. Ghosh, M. Das, P. Banerjee, S. Das, *Applied Surface Science* **254**(20), 6436 (2008).
- [26] W. Guang-Pu, Z. Zhi-Lin, Z. Wei-Ming, G. Xiang-Hong, C. Wei-Qun, H. Tanamura, H. Noguchi, T. Nagatomo, O. Omoto, *Conference Record of the IEEE Photovoltaic Specialists Conference* **1**, 365 (1994).
- [27] M. Patel, I. Mukhopadhyay, A. Ray, *Optical Materials* **35**(9), 1693 (2013).
- [28] D. Avellaneda, B. Krishnan, A. C. Rodriguez, T. K. Das Roy, S. Shaji, *Journal of Material Science* **26**, 5585 (2015).
- [29] S. J. Ikhmayies, Ph.D Thesis. University of Jordan, 2002.
- [30] S. J. Ikhmayies, R. N. Ahmad-Bitar, *Applied Surface Science* **255**(20), 8470 (2009).
- [31] A. Mukherjee, P. Mitra, *Materials Science-Poland* **33**(4), 847 (2015).
- [32] D. Prabha, S. Ilangovan, S. Balamurugan, M. Suganya, S. Anitha, V. S. Nagarethinam, A. R. Balu, *Optik* **142**, 301 (2017).
- [33] R. Mariappan, T. Mahalingam, V. Ponnuswamy, *Optik* **122**(24), 2216 (2011).
- [34] M. A. Manthrammel, M. Shkir, S. Shafik, M. Anis, S. AlFaify, *journal of materials research* **35**(4), 410 (2020).
- [35] F. Salamon, *International Letters of Chemistry, Physics and Astronomy* **64**, 1 (2016).
- [36] D. Shi, V. Adinolfi, R. Comin, M. Yuan, E. Alarousu, A. Buin, Y. Chen, S. Hoogland, A. Rothenberger, K. Katsiev, Y. Losovyj, X. Zhang, P. A. Dowben, O. F. Mohammed, E. H. Sargent, O. M. Bakr, *Science* **347**(6221), 519 (2015).
- [37] Y. Li, J. Wang, Y. Yuan, X. Donga, P. Wang, *Sustainable Energy & Fuels* **1**(5), 1041 (2017).
- [38] A. Bercegol, F. J. Ramos, A. Rebai, T. Guillemot, D. Ory, J. Rousset, L. Lombez, *The Journal of Physical Chemistry C* **122**(43), 24570 (2018).
- [39] X. Wen, R. Sheng, A. W. Y. Ho-Baillie, A. Benda, S. Woo, Q. Ma, S. Huang, M. A. Green, *The Journal of Physical Chemistry Letters* **5**(21), 3849 (2014).
- [40] S. S. Hegde, A. G. Kunjomana, K. A. Chandrasekharan, K. Ramesh, M. Prashantha, *Physica B: Condensed Matter* **406**(5), 1143 (2011).
- [41] N. K. Reddy, K. T. R. Reddy, *Thin Solid Films* **325**(1-2), 4 (1998).
- [42] W. Gu, F. Yang, C. Wu, Y. Zhang, M. Shi, X. Ma, *Nanoscale Research Letters* **9**(1), 662 (2014).

- [43] S. T. Navale, V. V. Mali, S. A. Pawar, R. S. Mane, M. Naushad, F. J. Stadler, V. B. Patil, *RSC Advances* **5**(64), 51961 (2015).
- [44] N. L. Tarwal, P. S. Patil, *Applied Surface Science* **256**(24), 7451 (2010).
- [45] H. Shintani, A. Sakudo, P. Burke, G. McDonnell, *Experimental and Therapeutic Medicine* **1**(5), 731 (2010).
- [46] S. D. Ferreira, W. S. Dernell, B. E. Powers, R. A. Schochet, C. A. Kuntz, S. J. Withrow, R. M. Wilkins, *Clinical Orthopaedics and Related Research* **388**, 233 (2001).
- [47] H. Shintani, N. Shimizu, Y. Imanishi, T. Sekiya, K. Tamazawa, A. Taniguchi, N. Kido, *Biocontrol Science* **12**(4), 13 (2007).
- [48] K.D. Weltmann, T. v. Woedtke, *Plasma Physics and Controlled Fusion* **59**(1), 014031 (2017).
- [49] J. Shen, Y. Tian, Y. Li, R. Ma, Q. Zhang, J. Zhang, J. Fang, *Scientific Reports* **6**(1), 28505 (2016).